Supplementary Information (SI) for Journal of Materials Chemistry C.

Two-Dimensional Lead-Free Double Perovskite for Self-powered and High Performance X-Ray Detection

Yongqiang Zhou[a], Lei Huang[a], Mengyue Wu[a], Faguang Kuang[d], Kang An[b], Peng Feng[b], Peng He[b,*], Yayun Pu[a,*], Jun'an Lai[b,*], Xiaosheng Tang[a,b,c,*]

[a] College of Optoelectronic Engineering, Chongqing University of Posts and Telecommunications, Chongqing, 400065, China.

[b] Key Laboratory of Optoelectronic Technology & Systems (Ministry of Education), College of Optoelectronic Engineering, Chongqing University, Chongqing 400044, China.

[c] School of Materials Science and Engineering, Zhengzhou University, Zhengzhou 450001, China.

[d] Key Laboratory of Human Brain bank for Functions and Diseases of Department of Education of Guizhou Province, College of Basic Medical, Guizhou Medical University, Guiyang 550025, China

*** Corresponding author**

E-mail: **penghe@cqu.edu.cn (P. He), puyy@cqupt.edu.cn (Y.Y. Pu), ja.lai@cqu.edu.cn (J. Lai), xstang@cqu.edu.cn (X.S. Tang)**

Experimental section

Chemical

Histamine dihydrochloride ($C_5H_{11}Cl_2N_3$, 99.999%), Silver chloride (AgCl, 99.95%), bismuth trioxide (Bi_2O_3, 99%), Hypophosphorous acid (H_3PO_2, 99.99%), Hydrobromic acid (HBr, 99.98%). All reagents are purchased from Adamas. All materials are commercially available and can be used without purification. Indium tin oxide coated glass (ITO glass) is bought from Yiyang South China Xiangcheng Technology Co., Ltd.

Synthesis of $(HA)_2AgBiBr_8$ Single Crystals

1.5 mmol of HACl (Histamine dihydrochloride, $C_5H_{11}Cl_2N_3$), 1.5 mmol of AgCl, and 0.75 mmolBi_2O_3 are hydrochloride in a mixture of 10 ml HBr and 2 ml H_2PO_2. It is then placed on a heating plate and stirred for 80ºC until completely dissolved, after which the solution is transferred to an absolutely clean lining. Set oven parameters Set the oven temperature to 180ºC, heating time for 4 h, then heat for 2 h, then cool down to room temperature, cooling time for 4 h, then heat up to 180ºC, heat preservation for 2h, 180ºC cooling to 100ºC for 72 h, 100ºC cooling to 20ºC for 72 h, heat preservation to 20ºC for 5h. Finally, the synthesized crystal is filtered out, washed with acetone (slightly soluble or insoluble and volatile solvent), and vacuumed for preservation.

Device Preparation

Before device fabrication, the $(HA)_2AgBiBr_8$ was cleaned three times with anhydrous ether, and then dried at 60 °C under a vacuum oven for 24 h. The $(HA)_2AgBiBr_8$ X-ray detector was made by depositing interdigital Ag electrodes (≈150 nm thickness) via vacuum evaporation.

Physical Characterization

The powder X-ray diffraction measurements (PXRD) were per-formed on PANalytical X’Pert Powder diffractometer. During the measurement, the Bragg’s diffraction angle (2°) range was set to 10° - 80° and scanning time is 20 min. Scanning electron microscopy (SEM) images were taken using Quattro S. Cold FE-SEM, Hitach

High-Technologies with an acceleration voltage of 10 KV, and EDX was used to characterize the elements of doping samples. Pure $(HA)_2AgBiBr_8$ was scanned by ZEISS GeminiSEM 300 field emission scanning electron microscope, and all elements were characterized by energy dispersive spectroscopy (EDS). The UV-Vis transmission spectra and absorption spectra were recorded with UV-3600 spectrophotometer (Shimadzu, Japan) in the wavelength range of 200 to 800 nm. The thermogravimetric analysis of crystals was performed by TGA/DSC1/1600LF (Mettler Toledo, Switzerland) at a heating rate of 20 °C/min up to 800 °C. The DFT calculation was performed on the Cambridge Sequential Total Energy Packge (CASTEP) module.

X-ray Detection: The I–V traces and I–t curves under X-ray irradiation were also recorded using the 6517B high-precision electrometer (Keithley, USA). A commercially available Ag target X-ray tube with photons energies as high as 50 KeV and peak intensity at 20 KeV was used as X-ray source (4 W, Mini-X2, Amptek, USA). The dose rate of the X-ray tube can be modulated via adjusting its tube current and measured using a commercial X-ray dosimeter (Accu-Gold, Radcal, USA) attached to the ion chamber (10X 6-180 model) in an integrating mode.

The optical band gap can be calculated by the following formula:[1]

$$(hvF(A))^{\frac{1}{n}} = A(hv - E_g) \quad (1)$$

Where F(A) is the absorption coefficient, hv is the photon energy, A is the proportionality constant, and E_g is the optical band gap.

Supplementary data section

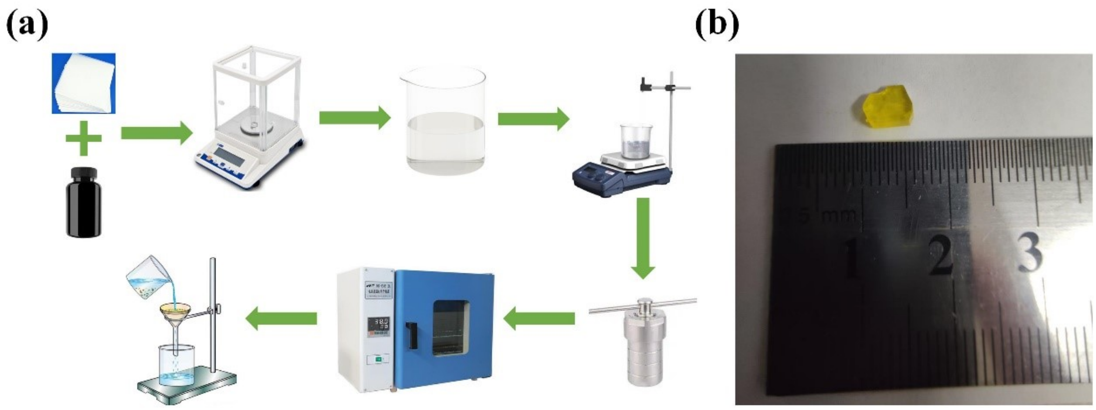

Figure S1. (a) Schematic diagram of preparing $(HA)_2AgBiBr_8$ crystal by hydrothermal method. (b) shows the growth of $(HA)_2AgBiBr_8$ crystal.

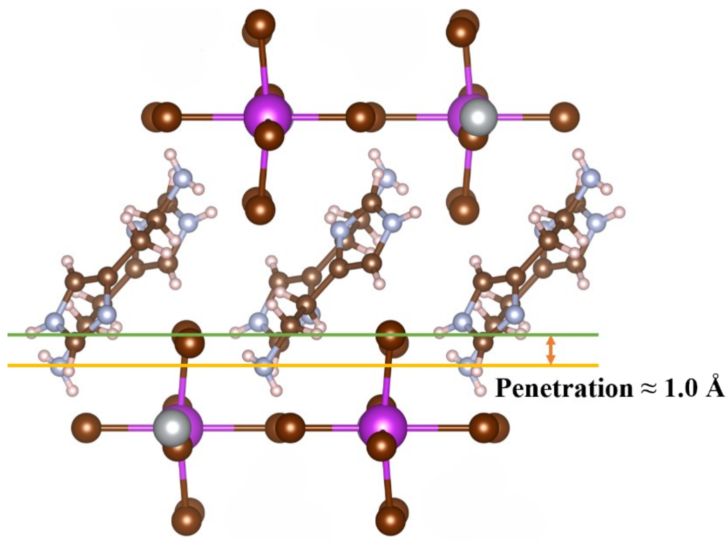

Figure S2. The distance between N atom in organic cation and terminal Br atom in inorganic layer (penetration depth).

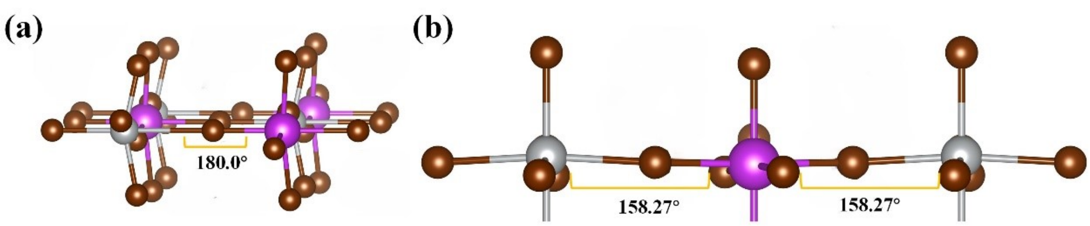

Figure S3. Equatorial Sb−Br−Ag bond angles of $(HA)_2AgBiBr_8$.

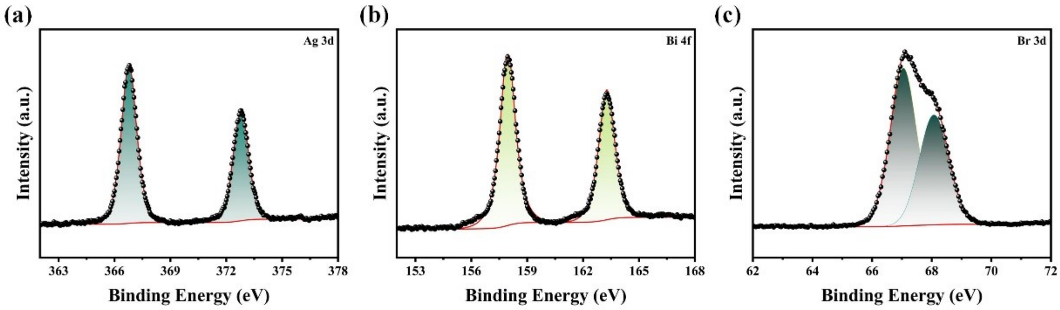

Figure S4. High resolution scans of (b) Ag, (c) Bi, (d)Br. All elements are in the expected valence states.

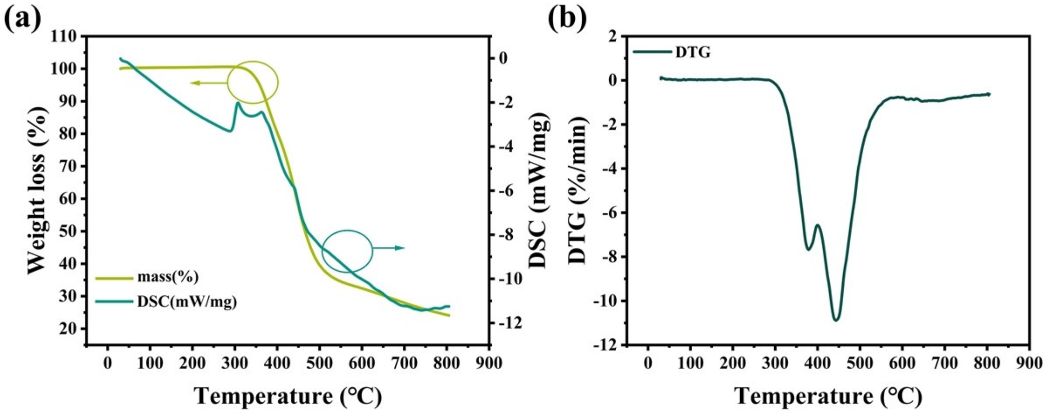

Figure S5. (a-b) Thermogravimetric analysis (TGA), Differential scanning calorimeter (DSC) and Derivative thermogravimetry **(**DTG) analysis of $(HA)_2AgBiBr_8$, powder under N_2 flowing atmosphere using a ramp rate of 20 °C/min from 30 to 800 °C.

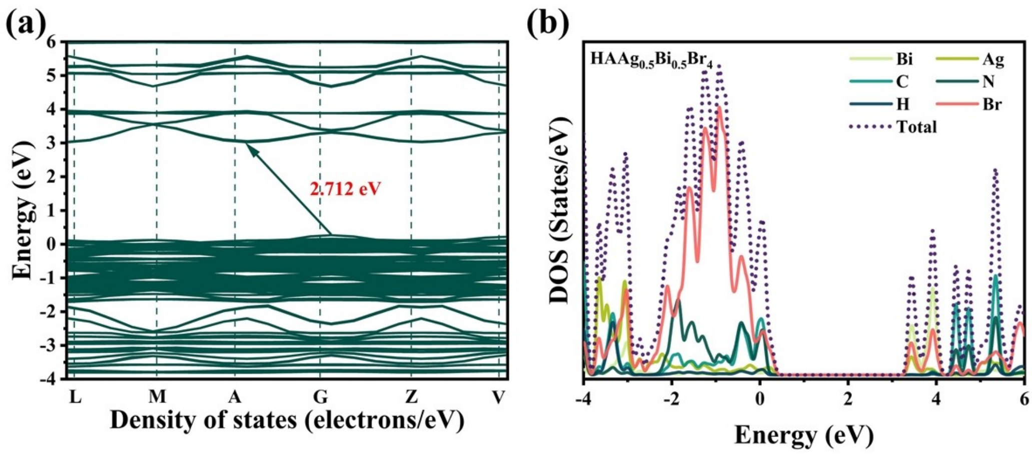

Figure S6. (a) Band structures for $(HA)_2AgBiBr_8$. (b) is the Total and projected density of states (DOS) of the states of $(HA)_2AgBiBr_8$.

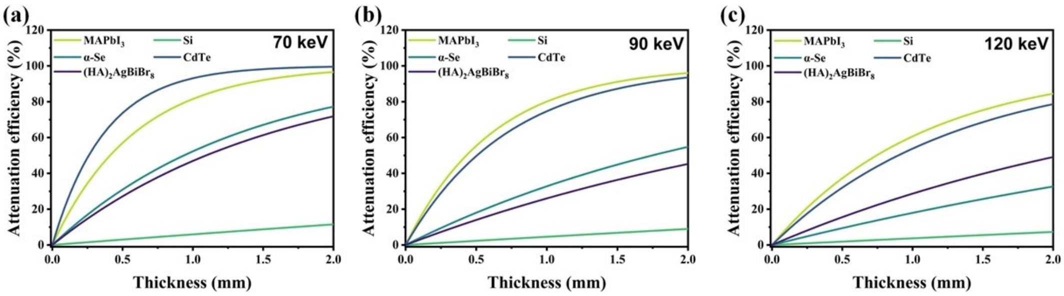

Figure S7. Attenuation efficiency of 70 KeV, 90KeV and 120KeV X-ray photons under different thicknesses for $(HA)_2AgBiBr_8$, Si, α-Se, CdTe and $MAPbI_3$.

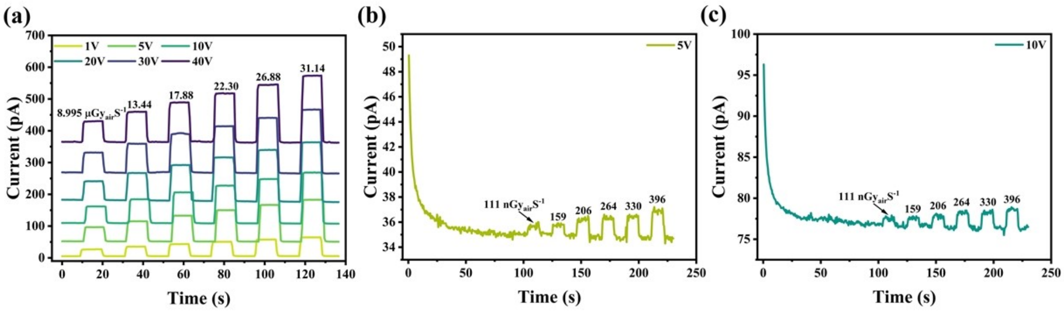

Figure S8. On/off photocurrent response of the $(HA)_2AgBiBr_8$ X-ray detector under different dose rates and at different bias voltage.

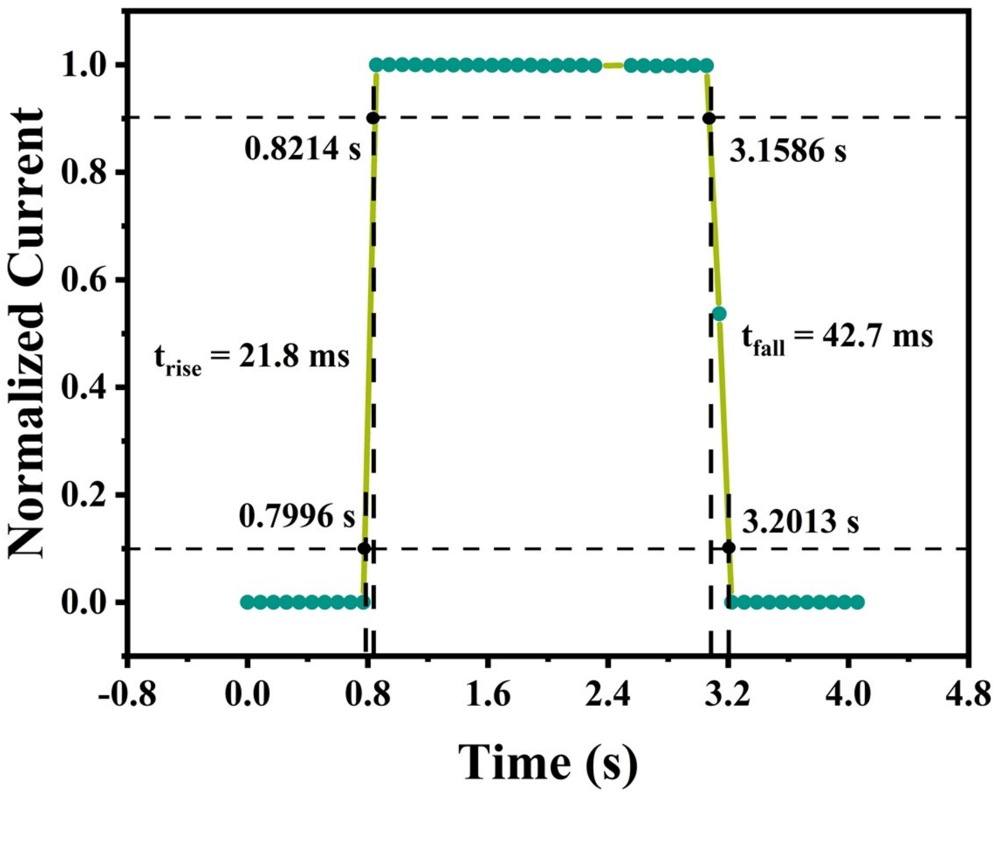

Figure S9. Rise and fall times of single-crystal $(HA)_2AgBiBr_8$ device.

Table S1. Single crystal X-ray diffraction data of $(HA)_2AgBiBr_8$ single crystals.

Compound	**$(HA)_2AgBiBr_8$**
Empirical formula	$C_5H_9Ag_{0.5}Bi_{0.5}Br_4N_3$
Formula weight	589.186
Temperature/K	200.15
Crystal system	monoclinic
space group	C2/c
a/Å	11.5526(5)
b/Å	12.1920(6)
c/Å	18.6749(9)
α/°	90
β/°	94.729(4)
γ/°	90
Volume/Å^3	2621.39(19)
Z	8
μ/mm^{-1}	19.652
F(000)	2097.7
ρ_{calc}g/cm^3	2.986

Table S2. Bond Angles for $(HA)_2AgBiBr_8$.

Atom	**Atom**	**Atom**	**Angle/°**	**Atom**	**Atom**	**Atom**	**Angle/°**
Br04^1	Bi01	Br04^2	178.16(6)	Br04^3	Ag02	Br03	90.78(4)
Br05	Bi01	Br04^1	90.92(3)	Br04	Ag02	Br03	88.03(4)
Br05	Bi01	Br04^2	90.92(3)	Br04	Ag02	Br04^3	173.95(8)
Br06	Bi01	Br04^2	89.08(3)	Br05	Ag02	Br03	101.41(5)
Br06	Bi01	Br04^1	89.08(3)	Br05	Ag02	Br03^3	101.41(5)
Br06	Bi01	Br05	180.0	Br05	Ag02	Br04	93.02(4)
Br07^3	Bi01	Br04^2	90.71(4)	Br05	Ag02	Br04^3	93.02(4)
Br07^3	Bi01	Br04^1	89.43(4)	Ag02^3	Br04	Bi01^4	158.27(6)

Br07	Bi01	Br04^{1}	90.71(4)	Ag02	Br05	Bi01	180.0
Br07	Bi01	Br04^{2}	89.43(4)	C00F	N008	C00B	109.2(12)
Br07^{3}	Bi01	Br05	85.51(3)	C00F	N00A	C00D	108.9(12)
Br07	Bi01	Br05	85.51(3)	C00D	C00B	N008	106.0(12)
Br07	Bi01	Br06	94.49(3)	C00E	C00B	N008	120.4(11)
Br07^{3}	Bi01	Br06	94.49(3)	C00E	C00B	C00D	133.6(13
Br07^{3}	Bi01	Br07	171.02(7)	C00E	C00C	N009	111.5(11)
Br07^{3}	Ag02	Br03	157.19(9)	C00B	C00D	N00A	107.8(13)
Br04	Ag02	Br03^{3}	90.78(4)	C00C	C00E	C00B	111.4(11)
Br04^{3}	Ag02	Br03^{3}	88.03(4)	N00A	C00F	N008	107.9(14)

Table S3. The chemical composition data measured by EDS of $(HA)_2AgBiBr_8$ crystal.

Element	Line Type	Wt%	Atomic percent
C	K	9.97%	42.28%
N	K	3.40%	12.35%
Br	L	54.35%	34.64%
Ag	L	12.56%	5.93%
Bi	M	19.72%	4.81%
Total		100%	100%

Table S4. Comparison of important X-ray parameters of different materials.

Type	Material	Sensitivity ($\mu CGy_{air}^{-1}m^{-2}$)	Electric Field (V/mm)	μτ-product (cm^2V^{-1})	detection limit ($\mu Gy_{air}s^{-1}$)	Ref.
RP	$(CPA)_4AgBiBr_8$	0.8	10	1×10^{-3}	-	2
RP	$(PMA)_2PbI_4$	283	555.6	8.05×10^{-3}	2.13	3
DJ	$(3AP)PbBr_4$	348.6	10	2.61×10^{-3}	3.04	4
DJ	$BDAPbI_4$	242	310	4.43×10^{-4}	0.43	5
RP	$(I\text{-}BA)_4AgBiI_8$	5.38	-	2.28×10^{-3}	500	6
RP	$(DFPIP)_4AgBiI_8$	188	-	1.1×10^{-5}	3.13	7
RP	$(BA)_2(MA)_2Pb_3I_{10}$	13	0	-	-	8
RP	$(BA)_2PbI_4$	1.48	10	4.5×10^{-3}	0.241	9
RP	$(BA)_2CsAgBiBr_7$	4.2	5	1.21×10^{-3}	70.5	10
DJ	**$(HA)_2AgBiBr_8$**	**252.38**	**24.84**	**2.047×10^{-3}**	**0.0689**	**This work**

Table S5. Response time and self-powering capability for reported perovskite-based X-ray detectors.

Material	Response time	self-powering capability	Ref.
$(4ABA)PbI_4$	110/190 ms	No	[11]
$(1,3\text{-}BMACH)PbBr_4$	-	Yes	[12]
$CsPbBr_3$ QDs film	30/27 ms	No	[13]
$MA_3Bi_2I_9$	23.3/31.4 ms	No	[14]
$(AMP)(MA)Pb_2I_7$	40/40 ms	Yes	[15]
BA_2PbBr_4	307/98 ms	No	[16]
$(BDA)(EA)_2Pb_3Br_{10}$	-	Yes	[17]
$(HA)_2AgBiBr_8$	**21.8/42.7 ms**	**Yes**	**This work**

References

1. P. Perfetti, C. Quaresima, C. Capasso, M. Capozi, F. Evangelisti, F. Boscherini and F. Patella, Electronic properties of the precrystallization regime of germanium: A photoemission study, *Physical review. B, Condensed matter*, 1986, **33**, 6998-7005.
2. W. Guo, X. Liu, S. Han, Y. Liu, Z. Xu, M. Hong, J. Luo and Z. Sun, Room-Temperature Ferroelectric Material Composed of a Two-Dimensional Metal Halide Double Perovskite for X-ray Detection, *Angewandte Chemie International Edition*, 2020, **59**, 13879-13884.
3. C.-X. Qian, M.-Z. Wang, S.-S. Lu and H.-J. Feng, Fabrication of 2D perovskite (PMA)2PbI4 crystal and Cu ion implantation improved x-ray detector, *Applied Physics Letters*, 2022, **120**, 011901.
4. C. Ma, L. Gao, Z. Xu, X. Li, X. Song, Y. Liu, T. Yang, H. Li, Y. Du, G. Zhao, X. Liu, M. G. Kanatzidis, S. F. Liu and K. Zhao, Centimeter-Sized 2D Perovskitoid Single Crystals for Efficient X-ray Photoresponsivity, *Chem. Mat.*, 2022, **34**, 1699-1709.
5. Y. Shen, Y. Liu, H. Ye, Y. Zheng, Q. Wei, Y. Xia, Y. Chen, K. Zhao, W. Huang and S. Liu, Centimeter-Sized Single Crystal of Two-Dimensional Halide Perovskites Incorporating Straight-Chain Symmetric Diammonium Ion for X-Ray Detection, *Angewandte Chemie International Edition*, 2020, **59**, 14896-14902.
6. Z. Xu, H. Wu, D. Li, W. Wu, L. Li and J. Luo, A lead-free I-based hybrid double perovskite (I-C4H8NH3)4AgBiI8 for X-ray detection, *Journal of Materials Chemistry C*, 2021, **9**, 13157-13161.
7. C.-F. Wang, H. Li, M.-G. Li, Y. Cui, X. Song, Q.-W. Wang, J.-Y. Jiang, M.-M. Hua, Q. Xu, K. Zhao, H.-Y. Ye and Y. Zhang, Centimeter-Sized Single Crystals of Two-Dimensional Hybrid Iodide Double Perovskite (4,4-Difluoropiperidinium)4AgBiI8 for High-Temperature Ferroelectricity and Efficient X-Ray Detection, *Adv. Funct. Mater.*, 2021, **31**, 2009457.
8. H. Tsai, F. Liu, S. Shrestha, K. Fernando, S. Tretiak, B. Scott, D. T. Vo, J. Strzalka and W. Nie, A sensitive and robust thin-film x-ray detector using 2D layered perovskite diodes, *Science Advances*, **6**, eaay0815.
9. Yukta, J. Ghosh, M. A. Afroz, S. Alghamdi, P. J. Sellin and S. Satapathi, Efficient and Highly Stable X-ray Detection and Imaging using 2D (BA)2PbI4 Perovskite Single Crystals, *ACS Photonics*, 2022, **9**, 3529-3539.
10. Z. Xu, X. Liu, Y. Li, X. Liu, T. Yang, C. Ji, S. Han, Y. Xu, J. Luo and Z. Sun, Exploring Lead-Free Hybrid Double Perovskite Crystals of (BA)2CsAgBiBr7 with Large Mobility-Lifetime Product toward X-Ray Detection, *Angewandte Chemie International Edition*, 2019, **58**, 15757-

15761.

11. Q. Fan, Y. Ma, S. You, H. Xu, W. Guo, Y. Liu, L. Tang, W. Li, J. Luo and Z. Sun, Dion–Jacobson Phase Perovskite Crystal Assembled by π-Conjugated Aromatic Spacer for X-Ray Detectors with an Ultralow Detection Limit, *Adv. Funct. Mater.*, 2024, **34**, 2312395.

12. D. Fu, Z. Chen, S. Wu, Y. Ma and X.-M. Zhang, Regulating the Stereoisomerism of Diammonium Cations to Construct Polar Dion-Jacobson Hybrid Perovskites for Self-Powered X-ray Detection, *Chem. Mat.*, 2024, **36**, 5284-5292.

13. J. Liu, B. Shabbir, C. Wang, T. Wan, Q. Ou, P. Yu, A. Tadich, X. Jiao, D. Chu, D. Qi, D. Li, R. Kan, Y. Huang, Y. Dong, J. Jasieniak, Y. Zhang and Q. Bao, Flexible, Printable Soft-X-Ray Detectors Based on All-Inorganic Perovskite Quantum Dots, *Adv. Mater. (Germany)*, 2019, **31**, 1901644.

14. X. Xu, W. Qian, S. Xiao, J. Wang, S. Zheng and S. Yang, Halide perovskites: A dark horse for direct X-ray imaging, *EcoMat*, 2020, **2**, e12064.

15. I.-H. Park, K. C. Kwon, Z. Zhu, X. Wu, R. Li, Q.-H. Xu and K. P. Loh, Self-Powered Photodetector Using Two-Dimensional Ferroelectric Dion–Jacobson Hybrid Perovskites, *J. Am. Chem. Soc.*, 2020, **142**, 18592-18598.

16. X. Xu, Y. Wu, Y. Zhang, X. Li, F. Wang, X. Jiang, S. Wu and S. Wang, Two-Dimensional Perovskite Single Crystals for High-Performance X-ray Imaging and Exploring MeV X-ray Detection, *ENERGY & ENVIRONMENTAL MATERIALS*, 2024, **7**, e12487.

17. H. Ye, Y. Peng, X. Shang, L. Li, Y. Yao, X. Zhang, T. Zhu, X. Liu, X. Chen and J. Luo, Self-Powered Visible-Infrared Polarization Photodetection Driven by Ferroelectric Photovoltaic Effect in a Dion–Jacobson Hybrid Perovskite, *Adv. Funct. Mater.*, 2022, **32**, 2200223.